ACS OMEGA

http://pubs.acs.org/journal/acsodf

Article

Electronic Effects of Support Doping on Hydrotalcite-Supported Iridium N-Heterocyclic Carbene Complexes

Kai Wang, Jonathan Horlyck, Matthew T. Finn, Marta Granollers Mesa, and Adelina Voutchkova-Kostal*

Cite This: https://doi.org/10.1021/acsomega.2c02593

Read Online

ACCESS | Metrics & More | Article Recommendations | Supporting Information

ABSTRACT: The electronic effects of supports on immobilized organometallic complexes impact their activity and lifetime, yet remain poorly understood. Here we describe a systematic study of the support effects experienced by an organometallic complex immobilized on doped hydrotalcite-like materials. To that end, we describe the synthesis and characterization of the first organometallic species immobilized on a palette of doped hydrotalcites via sulfonate linkers. The organometallic species consists of iridium *N*-heterocyclic carbene (NHC) carbonyl complex ([Na][Ir-(NHC-Ph-SO_3)$_2$(CO)$_2$]), a highly active molecular catalyst for transfer hydrogenation of glycerol. The hydrotalcite supports are composed of Al, Mg, and a compatible transition-metal dopant (Fe, Cu, Ni, Zn). The materials were characterized extensively by STEM, XPS, TGA, PXRD, FT-IR, N_2 desorption, ICP-AES, TPD, and microcalorimetry to probe the morphology and electronic properties of the support and elucidate structure−property relationships.

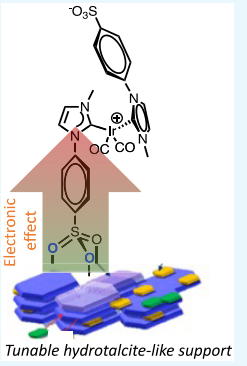

INTRODUCTION

Immobilized organometallic complexes (OM) as single-site species on high surface area supports are of significant interest in catalysis because they capture the advantages of both homogeneous and heterogeneous catalytic systems, including uniformity of active sites, high selectivity, robustness, easy recovery, use in flow reactors, and amenability to mechanistic studies.[1] While the growing number of reports of such catalysts attests to their potential,[2] adoption in industry has been stymied by a number of key challenges,[3] including inferior catalytic activity and selectivity relative to homogeneous precursors and leaching and/or decomposition that limits catalyst lifetime and recyclability. Optimization of catalytic activity and selectivity is challenging due to (a) formation of multiple ill-defined metal species and catalytic sites,[4] (b) unintended electronic effects and geometric constraints of the support on catalytic activity, and (c) nonselective activity of the support that interferes with the reaction of interest.[5] Leaching and decomposition are difficult to control as the mechanisms of decomposition to zerovalent metal nanoparticles are not fully elucidated.[6]

While the choice of catalyst supports has traditionally focused on nonreactive, or "innocent" materials, such as silica, γ-alumina, zeolites and polymers, we now appreciate that most (if not all) supports are in fact non-innocent in that they affect the electronic and steric properties of the immobilized complex and can participate in cooperative or independent reactions. To exploit the potential of non-innocent supports in development of immobilized catalysts, we must expand the molecular-level understanding of the complex surface chemistry. The latter demands systematic studies of model systems consisting of supports that allow controlled manipulation of acid−base properties and an organometallic precursor that can be immobilized robustly.

With these criteria in mind, we sought to study the electronic support effects of complex **1** (Figure 1), a compound designed in our group as a prolific catalyst for glycerol transfer hydrogenation and dehydrogenation.[7,8] The NHC ligands were selected for the precursor for two main reasons: first, we and others have shown Ir-NHC complexes to be active catalysts for dehydrogenation and transfer hydro-

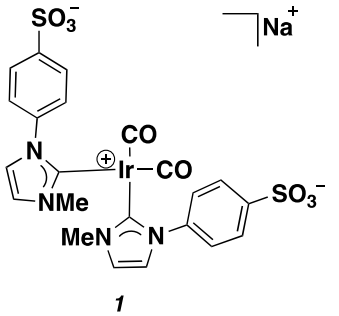

1

Figure 1. [Ir-(NHC-Ph-SO_3)$_2$-(CO)$_2$]Na.

Received: April 26, 2022
Accepted: June 21, 2022

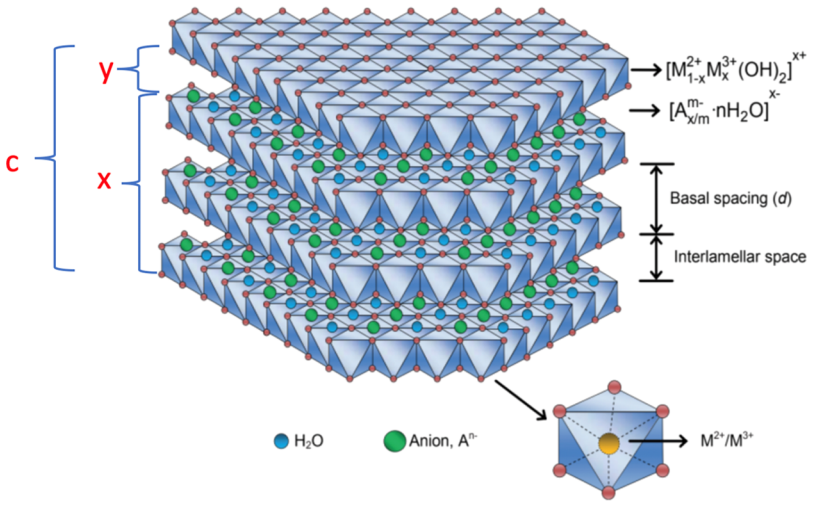

Figure 2. Schematic representation of layered double hydroxide structure of hydrotalcite, showing basal spacing d (003), approximately 4.8 Å,[10] PXRD parameter c = 3.d(003), and interlamellar space y (modified from Tronto et al.[15]).

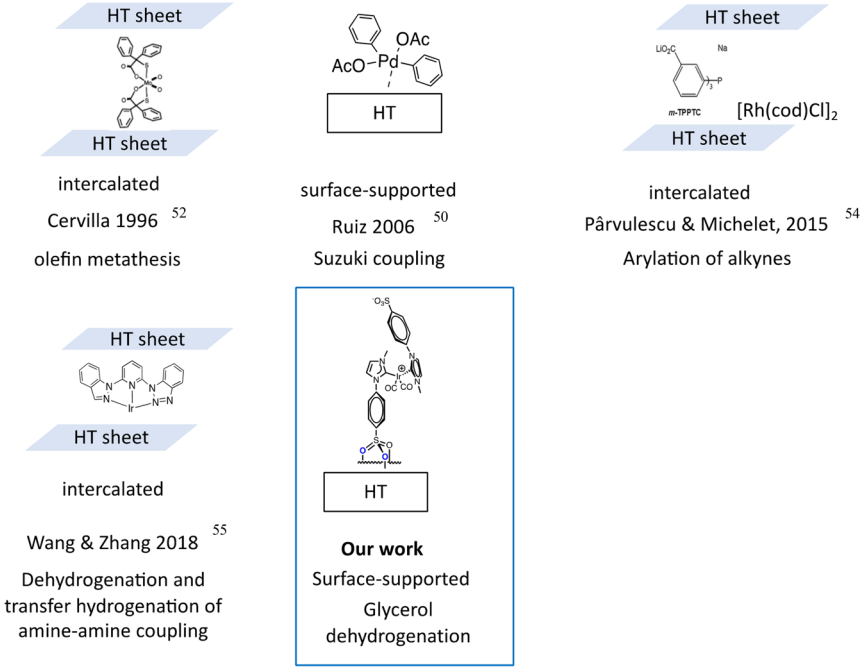

Figure 3. Hydrotalcite-supported immobilized catalysts.

genation processes, with higher activity than phosphine analogs; second, the thermal stability of NHC complexes exceeds that of phosphine analogs due to the higher bond dissociation energies of the latter.[9] The second factor is key when immobilizing on a support, where reactions with components of the surface can result in degradation.

The supports selected constitute a family of hydrotalcite-like materials (HTs), represented by formula $[M^{2+}_n M^{3+}_m(OH)_{2(m+n)}]^{m+}(An^{n-})_{m/x}\cdot yH_2O$, which can incorporate a range of M^{2+} and M^{3+} and anions (An^{n-}) (Figure 2).[10] The layered HT structure is composed of positively charged metal hydroxide layers charge-balanced by water and anions in the interlayer (most often carbonate). Surface hydroxyls serve as Brønsted basic sites, while cations (especially Al^{3+}) provide weak Lewis acidic sites. The acid and base properties of synthetic HTs can be easily tuned by (i) changing the M^{2+}:M^{3+} ratio,[11] (ii) varying the postsynthesis thermal treatment[12] (iii) altering the interlayer anions[13] (CO_3^{2-}, NO_3^-, $^tBu_3O^-$, Cl^-, oxalate) and (iv) doping with compatible M^{2+}, M^{3+} cations, namely, Ni^{2+}, Mn^{2+}, Fe^{3+}, Co^{2+}, Cu^{2+}, Zn^{2+}, and Cr^{3+}.[14] These tuning "knobs" allow one to selectively "dial in" electronic properties while maintaining relatively constant morphology and surface area.

While HTs have been extensively used as heterogeneous catalysts, their application as supports for organometallic species are limited to a few examples, most of which are intercalated in the hydrotalcite (Figure 3).[16−19] In one example, Ruiz et al.[20] suggested surface immobilization was achieved with a Pd, rather than interlayer intercalation, but without any multiatom linker that would favor surface binding. Here, we describe a systematic study of the support effects of organometallic complex **1** immobilized on doped hydrotalcites (HTs) via sulfonate linkers. We anticipate that this work will inform support effects on activity, selectivity and catalyst

https://doi.org/10.1021/acsomega.2c02593
ACS Omega XXXX, XXX, XXX−XXX

lifetime—insights critical to enabling the rational design of immobilized and single-site catalysts that overcome existing barriers to adoption by industry.

RESULTS AND DISCUSSION

Catalyst Synthesis and Characterization. Complex **1** was immobilized on a series of HTs, differing in dopant metal (Fe^{3+}, Zn^{2+}, Cu^{2+}, Ni^{2+}) and loading of precursor. Immobilization was performed using mesoscale continuous flow precipitation, whereby the support is precipitated in the presence of the organometallic precursor (Figure S2).[14] The latter process yields materials with reproducible electronic and morphological properties as well as precursor loading and dispersion.[14] The catalysts are denoted as **1**-x-HT[*n*], where *x* represents the transition-metal dopant of the HT and [*n*] denotes the mass percent loading of Ir. Five **1**-x-HT catalysts (x = none, Fe^{3+}, Zn^{2+}, Cu^{2+}, Ni^{2+}) were synthesized with <1 wt % loading of **1**. The low loading is intended to minimize potential agglomeration and maximize support interactions. To probe the effect of complex **1** loading on the support, three additional **1**-HT catalysts were synthesized with higher loadings of **1** and are denoted as **1**-x-HT [0.3%], **1**-x-HT [3%], and **1**-x-HT [6%], respectively. Elemental composition of the catalysts, determined by ICP-AES, shows small but reproducible differences in the loading of **1** obtained on HTs doped with different metals, ranging from 0.3 to 0.8 wt % (Table 1). However, the molar ratios of Mg:Al:x (where x is the dopant metal) in the HTs with and without the organometallic precursor are consistent (Table S2), suggesting minimal disruption of the HT matrix by precursor **1**.

Table 1. Elemental Composition of 1-x-HT[*n*] catalysts (x = none, Cu, Ni, Zn, and Fe) from ICP-AES

1-x-HT[*n*]	Ir (wt %)	molar ratio Mg/Al/M	Al^{3+} (wt %)	Mg^{2+} (wt %)	x (wt %)
1-Cu-HT [0.4%]	0.38	51/36/13	7.48	9.53	6.14
1-Ni-HT [0.4%]	0.37	51/32/17	9.18	13.1	10.9
1-Fe-HT [0.8%]	0.77	41/37/22	10.8	10.8	13.3
1-Zn-HT [0.3%]	0.25	50/30/20	9.49	14.8	15.6
1-HT [0.3%]	0.26	68/32/0	10.5	20.0	
1-HT [1%]	1.16	68/31/0	9.25	18.3	
1-HT [3%]	3.10	65/32/0	9.36	18.05	
1-HT [6%]	5.60	77/17/0	8.88	16.12	
$IrCl_3$–HT[12%]	12.0	77/17/0	5.44	22.4	12.0

The surface area (S_{BET}) of the catalysts and HT supports, determined by the BET method, was in the range of 93−148 m^2/g for the HT supports and 98−203 m^2/g for the immobilized **1**-xHTs (Table S3). The variance in S_{BET} for the catalysts is consistent with that observed in HTs with different dopant metals. The catalysts are mesoporous, with relatively narrow pore size distributions in the range of 3−12 nm (Figure S3).

Powder X-ray diffraction (PXRD) of the catalysts confirmed the presence of HT phase, characterized by (003), (006), (009), (015), (018), (110), and (113) reflections (Figure 4).[14] Immobilization of **1** also has a negligible effect on the crystalline structure of the HTs (Figures S4−S8), with consistent *a* and *c* parameters observed regardless of metal dopant (Table S4). The fact that interlamellar spacing does not increase significantly with immobilization, even at the 3% loading of **1**, suggests that immobilization likely occurs on the support surface. Further evidence for surface immobilization comes from atomic force microscopy (AFM) studies of sulfonate complexes on HTs.[21] However, PXRD evidence cannot rule out potential of some intercalation of complex **1** at low catalyst loadings.

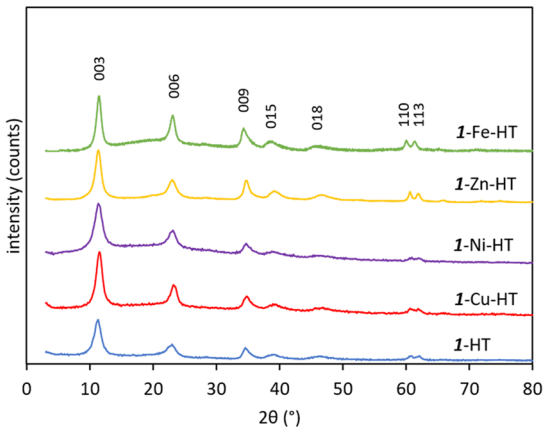

Figure 4. PXRD patterns of **1**-x-HT[*c*] catalysts (x = none, Cu, Ni, Zn and Fe; *c* < 1%).

Scanning transmission electron microscopy with energy-dispersive X-ray spectroscopy (STEM-EDS) images of **1**-x-HTs show uniform distribution of Mg, Al, dopant metal, and Ir with no segregated nanoparticle formation, except in the case of **1**-Cu-HT (Figure 5), which exhibits nanoparticles with size

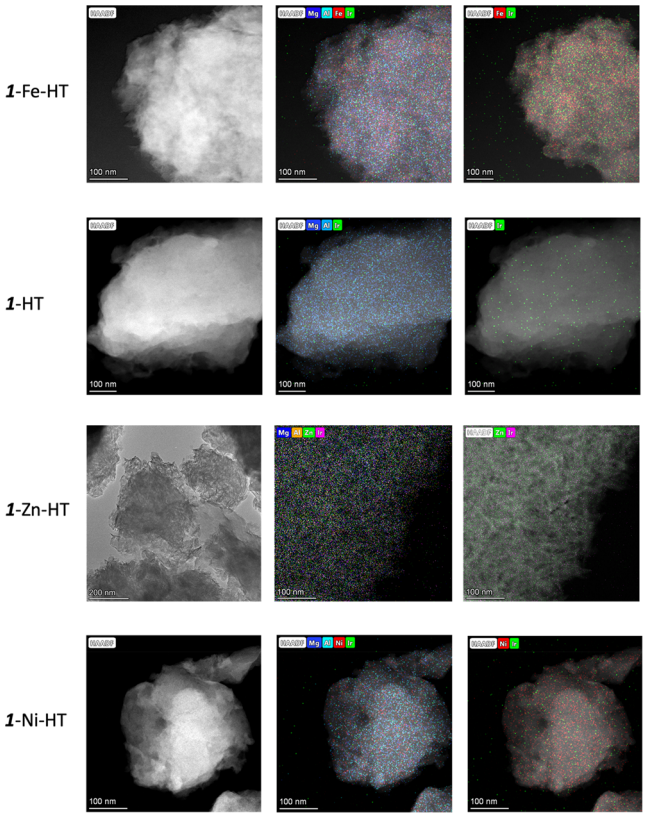

Figure 5. STEM-EDS images and elemental analysis of 1-x-HT (x = Fe, Zn, Ni, none).

https://doi.org/10.1021/acsomega.2c02593
ACS Omega XXXX, XXX, XXX−XXX

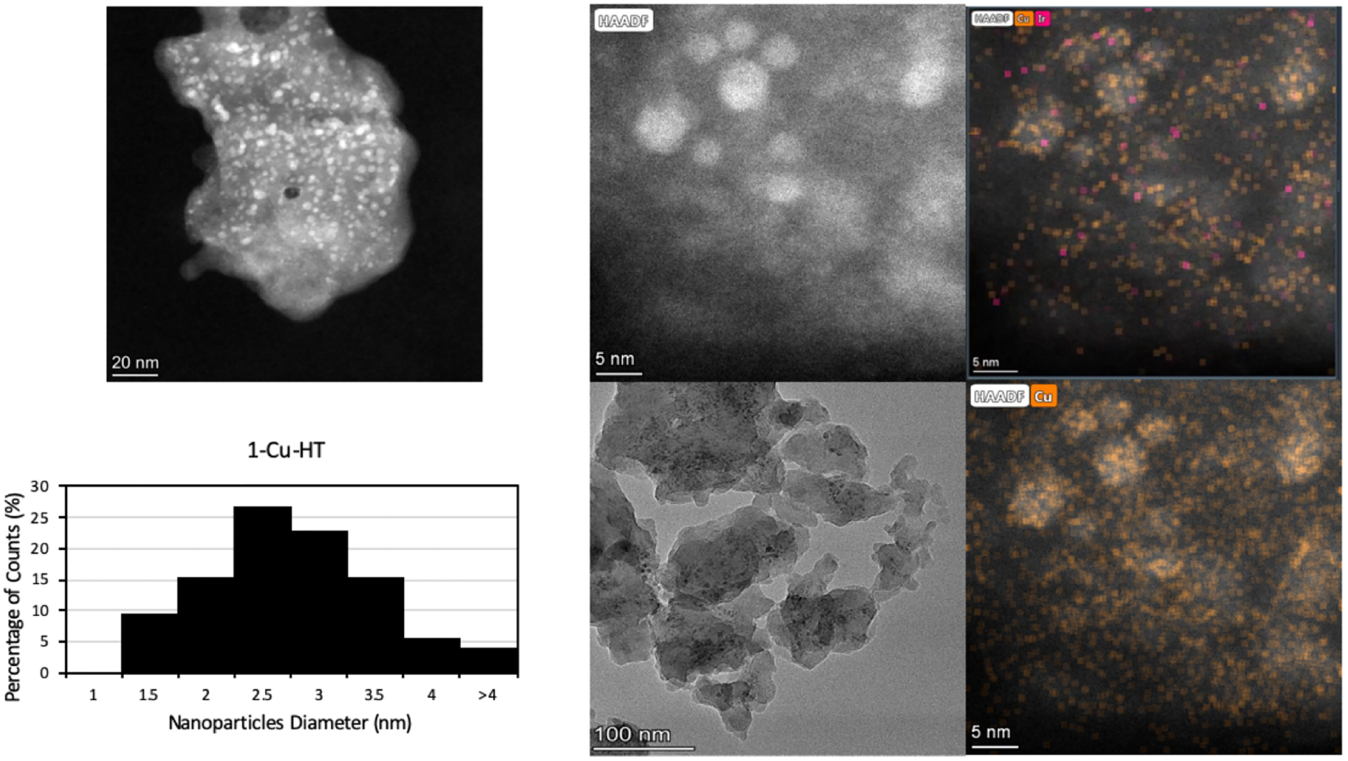

Figure 6. TEM and STEM-EDS images of **1**-Cu-HT with NP size distribution.

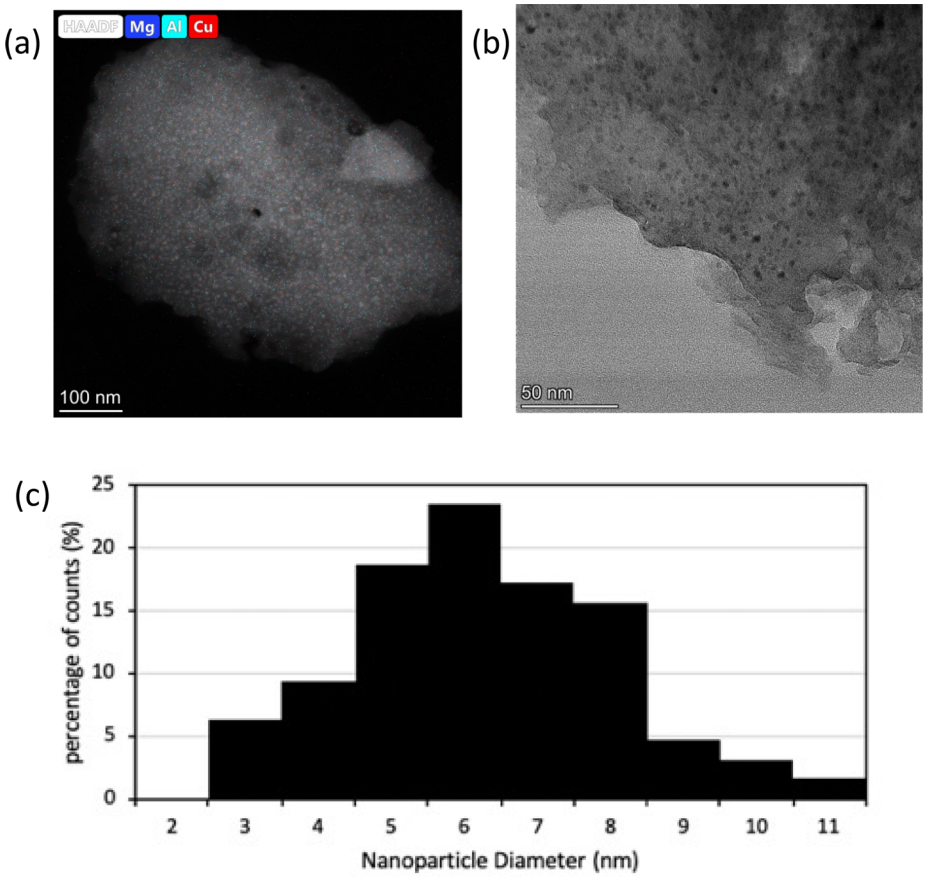

Figure 7. (a) STEM-EDS and (b) TEM image of Cu-HT without **1** and (c) nanoparticle size distribution of the latter.

distribution 1−5 nm. EDS mapping confirms that these nanoparticles consist of a more concentrated Cu phase, with well-dispersed iridium across the surface (Figure 6). The formation of Cu-based nanoparticles is not surprising, given

https://doi.org/10.1021/acsomega.2c02593
ACS Omega XXXX, XXX, XXX−XXX

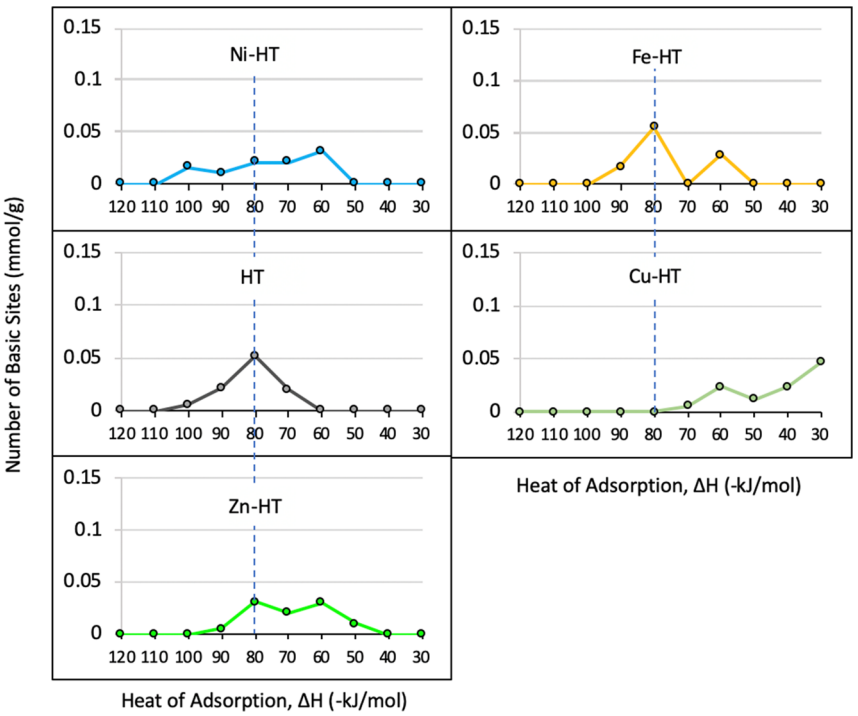

Figure 8. Distribution of the interaction strengths for CO_2 adsorption on x-HT from microcalorimetry.

that copper ions cause greater disorder in the layered double hydroxide lattice relative to the other dopants due to their larger ionic radii compared to that of Mg^{2+}; the latter makes them prone to phase separation. Notably, Cu-HT without **1** also shows phase separation by STEM (Figure 7). However, no copper phase was observed by PXRD, which is consistent with highly dispersed and poorly crystalline copper NPs.

In order to evaluate the basic site distribution of doped HT supports, the surface basicity was examined using microcalorimetry data with CO_2 as an acid probe.[22] Microcalorimetry affords plots of the differential enthalpy of adsorption as a function of coverage for the adsorption of CO_2 (Figure S-9), which was used to calculate the relative abundance of sites that physisorb or chemisorb CO_2 vs heats of adsorption (DH), as shown in Figure 8. Heats of adsorption lower than −80 kJ/mol reflect chemisorption, while those greater than that indicate threshold−physisorption.[23] The distribution of basic sites derived from those plots is clearly influenced by the dopant metal of the HT. Based on total basicity, defined based on chemisorption of CO_2, the trend of basicity of doped HTs, from highest to lowest is

Ni−HT > HT ~ Fe-HT > Zn-HT > Cu-HT

The basicity of the immobilized catalysts was also determined by CO_2 temperature-programmed desorption (TPD). A limitation of this technique for these catalysts is that to eliminate interference from carbonate ions in the interlayer, which thermally decompose to CO_2, samples were precalcined. While calcination is known to increase the basicity of hydrotalcite materials, we anticipated that it will likely not alter the relative basicity trend of the hydrotalcites. TPD of the calcined catalysts suggests the presence of basic sites of weak strength (CO_2 desorption at 50−200 °C) and moderate strength (200−400 °C), as shown in Figure 9a. The overall basicity can be determined by the relative number of basic sites, resulting in the following trend:

1-Ni-HT > **1**-HT > **1**-Cu-HT ≈ **1**-Zn-HT > **1**-Fe-HT

Among these, **1**-Ni-HT and **1**-HT have the highest relative number of moderate basic sites. **1**-Ni-HT also has the highest relative number of weak basic sites. While the trends in basicity are reasonably consistent between the two techniques, it is likely that the increase in basicity which occurs upon

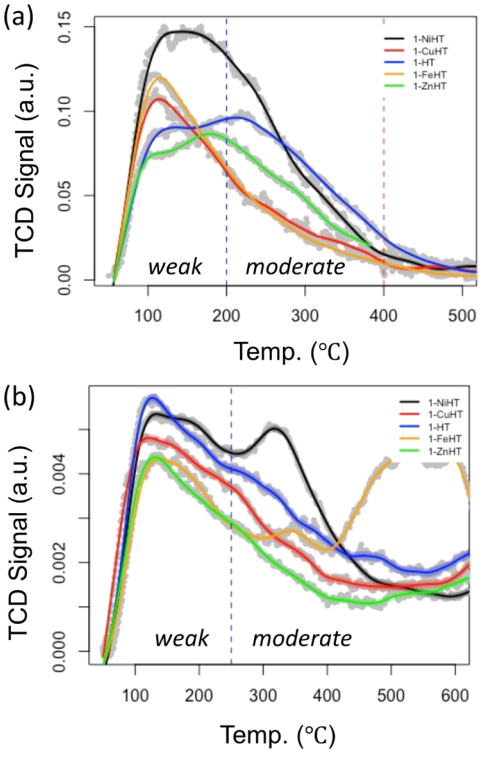

Figure 9. Temperature-programmed desorption (TPD) profiles with (a) CO_2 and (b) NH_3 of the **1**-x-HTs.

https://doi.org/10.1021/acsomega.2c02593
ACS Omega XXXX, XXX, XXX−XXX

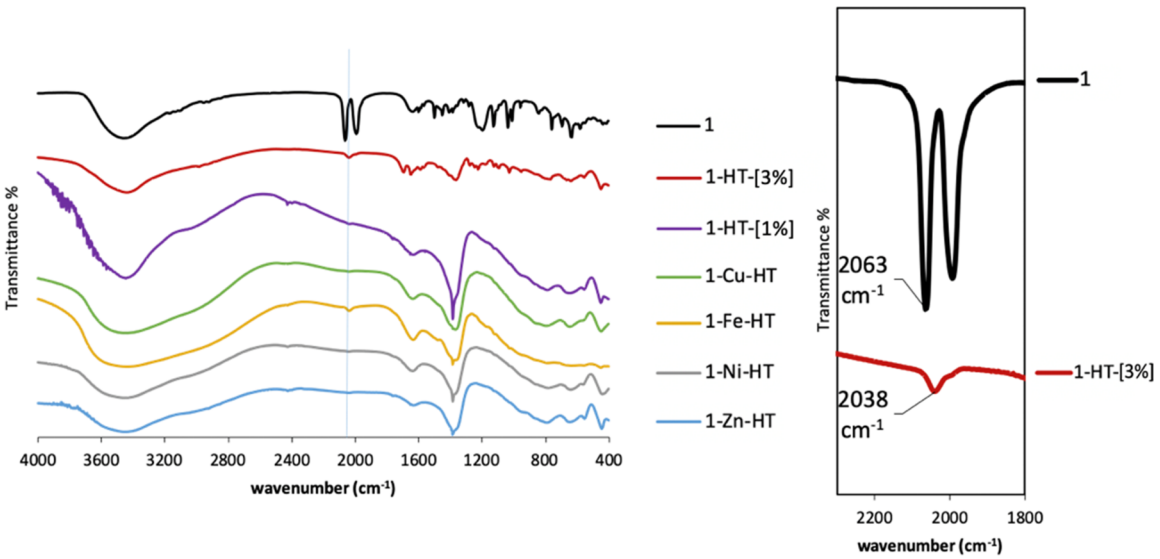

Figure 10. FTIR of complex **1** and **1**-x-HT catalysts (x = none, Cu, Ni, Zn, and Fe) highlighting the carbonyl stretching (υ_{co}) region.

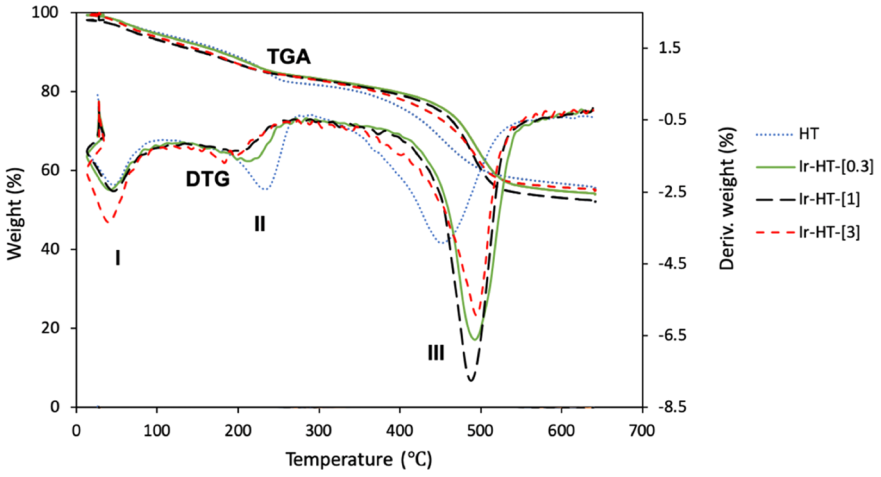

Figure 11. TGA-DTA curves for HT and **1**-HT[c] where c = 0.3%, 1%, and 3%.

calcination is higher for Cu-HT and Zn-HT than for Fe-HT. To further substantiate this argument, we characterized HTs after ex situ heating analogous to that incurred during TPD measurement and show that this results in significant changes in structure, as evidenced by increased surface area (BET) and change in PXRD patterns consistent with mixed metal oxide phase.

The acidity of the calcined catalysts was explored with NH_3 TPD, and the TPD profiles are shown in Figure 9b. All **1**-HTs show comparable broad asymmetric desorption features at 100 °C to ∼400 °C, corresponding to weak acidic sites. **1**-Ni-HT and **1**-Fe-HT also show a second feature with maxima at 320 and ∼480−600 °C, respectively, corresponding to moderate acidic sites. The major features of the CO_2 and NH_3 TPD profiles are consistent with those reported for other modified hydrotalcites.[24,25]

FT-IR spectra of **1**-x-HTs show characteristic bands for carbonate anions (1350−1370 cm^{-1}) and interlayer water (∼1400 and 1700 cm^{-1}, Figure 10) within HTs.[26,27] Although most of the IR features of precursor **1** are indistinguishable at low catalyst loadings in the immobilized catalysts, the carbonyl (CO) stretches (υ_{co}) were intense enough to be identified in all five materials. Given that the υ_{co} of iridium carbonyl complexes provides an indirect probe of relative electron density of the metal,[8,28] the differences in υ_{co} should correspond to electronic effects of the support on the complex, assuming that the complex is immobilized intact and in the same form on each doped HT support. The experimental υ_{co} stretches of free complex **1** (2063 and 1992 cm^{-1}) were identified using DFT calculations as the symmetric and asymmetric stretch, respectively (Table S5). After immobilization of **1** on HTs, the more intense symmetric υ_{co} at 2063 cm^{-1} red-shifted by ∼25 cm^{-1} to 2038 cm^{-1} (Figure 10), which suggests that the immobilized complex is more electron-rich relative to the precursor. The latter stretch showed little variation for **1**-x-HTs doped with Cu, Ni, Fe, and Zn (2036−2040 cm^{-1}, Table S7), suggesting that metal doping of the support does not quantifiably impact the electronics of immobilized complex. While the above data strongly suggests that the immobilized carbonyl complexes on all the supports are structurally consistent, it does not exclude the possibility that upon immobilization the complex structure changes, for example by dissociation of one CO. Such structural detail is challenging to ascertain, although further modeling efforts are underway to elucidate this in the future.

https://doi.org/10.1021/acsomega.2c02593
ACS Omega XXXX, XXX, XXX−XXX

The thermal decomposition of **1**-HT was studied to elucidate changes to stability upon immobilization at 0.3%, 1%, and 3% loadings. All three catalysts exhibit the characteristic thermal decomposition profiles of hydrotalcites with three endothermic transitions: (I) loss of physiosorbed water below 100 °C; (II) loss of interlayer water and carbonates at ∼150−250 °C; and (III) and dehydroxylation and decarbonation at 350−550 °C (Figure 11).[29] Immobilization of **1** increases the temperature of transition III from ∼420 to 488−495 °C in **1**-HT, with negligible loading dependence of **1** (Figure S10). Meanwhile, the temperature of interlayer water loss (region II) decreases with a more evident loading dependence on **1**. Thus, immobilization of **1** decreases the stability of surface water and increases the stability of carbonate/waters in the interlayer. This trend could be the result of: (i) change in charge distribution of the HT upon immobilization of **1**, possibly by intercalation of some complex **1** in the interlayers, which translates to a change in the Coulombic interactions between interlayer water and the cationic sheets of the HT, or (ii) blocking of some micropores by complex **1**.

The stability of the local structure of the immobilized species, and the effect of the support on the latter stability, is an important facet of the potential catalytic utility of these materials. Ultimately, the most direct evidence for the stability of the catalytic species is obtained from kinetic studies using the catalysts in a continuous flow reactor. Such a study on the dehydrogenative conversion of glycerol to lactic acid by the latter materials was performed and detailed in an adjacent study,[30] showing that materials retain their catalytic reaction rate for over 20 h on stream at 225 °C.

X-ray photoelectron spectroscopy (XPS) analysis of **1** and **1**-x-HTs confirms the Ir $4f_{7/2}$ and $4f_{5/2}$ binding energies (∼62.1 and 65.1 eV, respectively), consistent with a single Ir(I) species (Figure 12a).[31] Only in the case of **1**-Cu-HT do we observe an additional feature at ∼61.0 and 64.1 eV, consistent with a second Ir(0) species.[32] Additional features consistent with Cu^{2+} and Cu^{1+}/Cu^{0} are seen in the Cu 2p region[33] (Figure 12b).

To unequivocally identify the structure of immobilized complex **1**, we attempted to collect the cross-polarized magic angle spinning (CP-MAS) solid-state NMR spectra for the highest loading catalyst (**1**-HT [6%]). However, even at this loading, the concentration of **1** was too low to obtain ^{1}H or ^{13}C spectra with sufficient resolution to gain structurally meaningful information. While we hope to be able to address this shortcoming in the future, the extensive set of spectroscopic characterizations performed is consistent with the current assertion that **1** is intact and on the surface of HT as the major species.

CONCLUSION

Advances in our ability to design active and robust single-site heterogeneous catalysts that take advantage of synergistic activity of acid−base supports requires the elucidation of the electronic effects the supports exert on the immobilized species. Here, we report the design and characterization of novel supported catalysts consisting of Ir(I) *N*-heterocyclic carbene complex (**1**) immobilized on hydrotalcite-like materials (HTs) via sulfonate linkers. The HT supports are layered double hydroxides composed of Al, Mg, and a transition-metal dopant x (x = Fe, Cu, Ni, Zn). The use of doped hydrotalcites as catalytic supports for potential single-

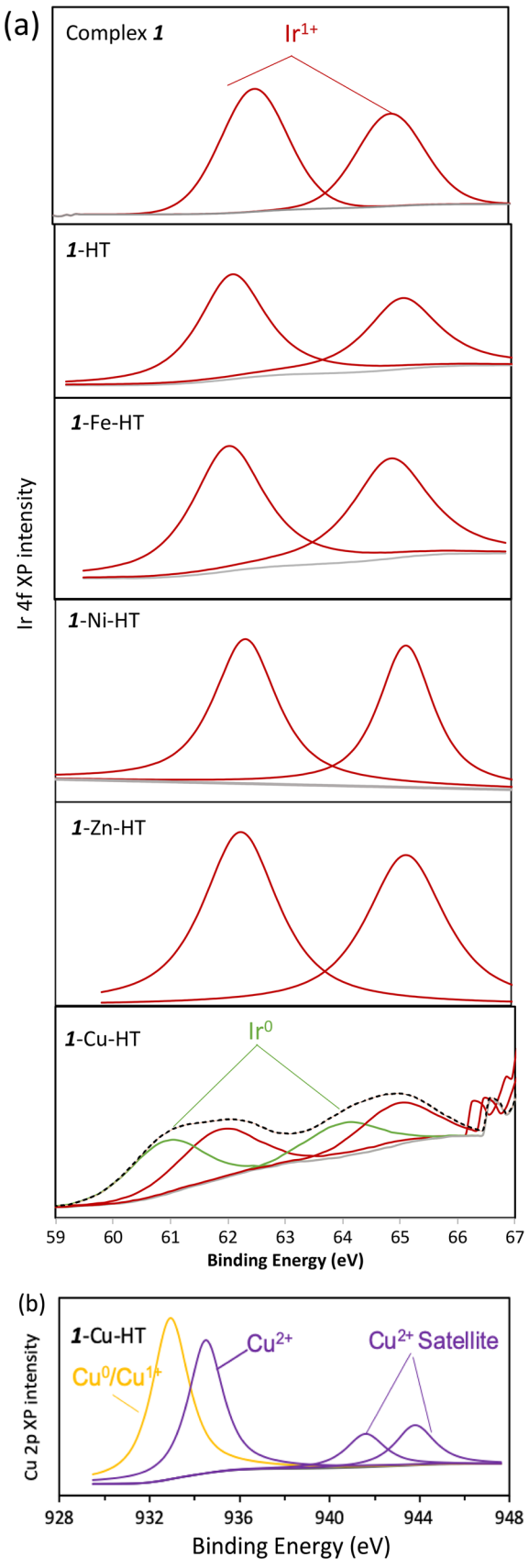

Figure 12. (a) Ir 4f X-ray photoelectron spectra of complex **1** and **1**-x-HT[*c*] catalysts (x = none, Cu, and Fe; *c* < 1%) and (b) Cu 2p X-ray photoelectron spectrum of **1**-Cu-HT.

https://doi.org/10.1021/acsomega.2c02593
ACS Omega XXXX, XXX, XXX−XXX

site catalysts is highly promising due to the tunable acid−base properties of these materials, the robust linkage to sulfonate-functionalized organometallic complexes, the reproducible one-step support coprecipitation and catalyst immobilization procedure, as well as the potential synergistic action of hydrotalcites in multistep catalytic processes. In order to evaluate the basic site distribution of doped HT supports, the surface basicity was examined using microcalorimetry and CO_2 temperature-programmed desorption (TPD). The distribution of basic sites on the support is influenced by the dopant metal of the HT and follows the trend Ni-HT > HT ∼ Fe-HT > Zn-HT > Cu-HT. Extensive characterization of the catalysts using ICP-AES, PXRD, FTIR, XPS, BET, and STEM suggests highly dispersed surface immobilization of Ir-NHC complex **1** and a substantial electronic effect on the iridium upon immobilization but a negligible difference upon support doping. Only in the case of immobilization of **1** on Cu-HT do we observe small Cu nanoparticles, but with no iridium enrichment, suggesting iridium and copper are not conforming core−shell nanoparticles. We anticipate that this work will highlight the support effects on activity, selectivity and catalyst lifetime—insights critical to enabling the rational design of immobilized and single-site catalysts that overcome existing barriers to adoption by industry.

■ ASSOCIATED CONTENT

Supporting Information

The Supporting Information is available free of charge at https://pubs.acs.org/doi/10.1021/acsomega.2c02593.

Catalyst synthesis, characterizations, and NMR characterization of compounds (PDF)

■ AUTHOR INFORMATION

Corresponding Author

Adelina Voutchkova-Kostal − *Department of Chemistry, The George Washington University, Washington, DC 20052, United States;* orcid.org/0000-0002-7016-5244; Email: avoutchkova@gwu.edu

Authors

Kai Wang − *Department of Chemistry, The George Washington University, Washington, DC 20052, United States;* orcid.org/0000-0002-3225-6559

Jonathan Horlyck − *Department of Materials Science and Engineering, Johns Hopkins University, Baltimore, Maryland 21218, United States;* orcid.org/0000-0003-2417-9044

Matthew T. Finn − *Department of Chemistry, The George Washington University, Washington, DC 20052, United States;* orcid.org/0000-0001-9474-7022

Marta Granollers Mesa − *Energy and Bioproducts Research Institute (EBRI), Aston University, Birmingham B4 7ET, United Kingdom;* orcid.org/0000-0001-8602-9362

Complete contact information is available at: https://pubs.acs.org/10.1021/acsomega.2c02593

Funding

We thank the NSF for funding this work through NSF CAREER award 1554963.

Notes

The authors declare no competing financial interest.

■ ACKNOWLEDGMENTS

We would thank th eNSF for funding this work through NSF CAREER award 1554963 as well as the Cahill and Wagner groups at GWU for use of PXRD, TGA, and BET instrumentation.

■ REFERENCES

(1) Thomas, J. M.; Raja, R.; Lewis, D. W. Single-site heterogeneous catalysts. *Angew. Chem., Int. Ed.* **2005**, *44* (40), 6456−6482.

(2) Pelletier, J. D. A.; Basset, J. M. Catalysis by Design: Well-Defined Single-Site Heterogeneous Catalysts. *Acc. Chem. Res.* **2016**, *49* (4), 664−677.

(3) Hübner, S.; de Vries, J. G.; Farina, V. Why Does Industry Not Use Immobilized Transition Metal Complexes as Catalysts? *Adv. Synth. Catal.* **2016**, *358* (1), 3−25.

(4) McKittrick, M. W.; Jones, C. W. Toward single-site, immobilized molecular catalysts: Site-isolated Ti ethylene polymerization catalysts supported on porous silica. *J. Am. Chem. Soc.* **2004**, *126* (10), 3052−3053.

(5) Huang, Z.; Brookhart, M.; Goldman, A. S.; Kundu, S.; Ray, A.; Scott, S. L.; Vicente, B. C. Highly Active and Recyclable Heterogeneous Iridium Pincer Catalysts for Transfer Dehydrogenation of Alkanes. *Adv. Synth. Catal.* **2009**, *351* (1−2), 188−206.

(6) Schmidt, A. F.; Al-Halaiqa, A.; Smirnov, V. V. Heck reactions of alkenes with aryl iodides and aryl bromides: Rate-determining steps deduced from a comparative kinetic study of competing and noncompeting reactions. *Kinet. Catal.* **2007**, *48* (5), 716−727.

(7) Finn, M.; Ridenour, J. A.; Heltzel, J.; Cahill, C.; Voutchkova-Kostal, A. Next-Generation Water-Soluble Homogeneous Catalysts for Conversion of Glycerol to Lactic Acid. *Organometallics* **2018**, *37* (9), 1400−1409.

(8) Ainembabazi, D.; Wang, K.; Finn, M.; Ridenour, J.; Voutchkova-Kostal, A. Efficient transfer hydrogenation of carbonate salts from glycerol using water-soluble iridium N-heterocyclic carbene catalysts. *Green Chem.* **2020**, *22* (18), 6093−6104.

(9) Segaud, N.; Johnson, C.; Farre, A.; Albrecht, M. Exploring the stability of the NHC-metal bond using thiones as probes. *Chem. Commun.* **2021**, *57* (81), 10600−10603.

(10) Cavani, F.; Trifiro, F.; Vaccari, A. Hydrotalcite-Type Anionic Clays: Preparation, Properties and Applications. *Catal. Today* **1991**, *11* (2), 173−301.

(11) Xie, W. L.; Peng, H.; Chen, L. G. Calcined Mg-Al hydrotalcites as solid base catalysts for methanolysis of soybean oil. *J. Mol. Catal. A-Chem.* **2006**, *246* (1−2), 24−32.

(12) Sahu, P. K.; Sahu, P. K.; Gupta, S. K.; Agarwal, D. D. Role of calcinations and basicity of hydrotalcite as catalyst for environmental benign novel synthesis of 4H-pyrimido[2,1-b][1,3]benzothiazole derivatives of curcumin. *Catal. Sci. Technol.* **2013**, *3* (6), 1520−1530.

(13) Valente, J. S.; Figueras, F.; Gravelle, M.; Kumbhar, P.; López, J.; Besse, J. P. *J. Catal.* **2000**, *189*, 370.

(14) Yaseneva, P.; An, N.; Finn, M.; Tidemann, N.; Jose, N.; Voutchkova-Kostal, A.; Lapkin, A. Continuous synthesis of doped layered double hydroxides in a meso-scale flow reactor. *Chem. Eng. J.* **2019**, *360*, 190−199.

(15) Tronto, J.; Bordonal, A. C.; Naal, Z.; Valim, J. B. Conducting polymers/layered double hydroxides intercalated nanocomposites. *Mater. Sci.* **2013**, 3−30.

(16) Cervilla, A.; Llopis, E.; Ribera, A.; Corma, A.; Fornés, V.; Rey, F. Intercalation of the oxo-transfer molybdenum(VI) complex [MoO2{O2CC(S) Ph2}2]2− into a zinc(II)−aluminium(III) layered double hydroxide host. Catalysis of the air oxidalton of thiols. *J. Chem. Soc., Dalton Trans.* **1994**, No. 20, 2953−2957.

(17) Moreno, M.; Ana, M. A. S.; Gonzalez, G.; Benavente, E. Poly(acrylonitrile)-montmorillonite nanocomposites: Effects of the intercalation of the filler on the conductivity of composite polymer electrolytes. *Electrochim. Acta* **2010**, *55* (4), 1323−1327.

(18) Neaţu, F.; Ciobanu, M.; Ştoflea, L. E.; Frunză, L.; Pârvulescu, V. I.; Michelet, V. Arylation of alkynes over hydrotalcite docked Rh-m-TPPTC complex. *Catal. Today* **2015**, *247*, 155−162.
(19) Ge, C.; Sang, X.; Yao, W.; Zhang, L.; Wang, D. Unsymmetrical indazolyl-pyridinyl-triazole ligand-promoted highly active iridium complexes supported on hydrotalcite and its catalytic application in water. *Green Chem.* **2018**, *20* (8), 1805−1812.
(20) Jiménez-Sanchidrián, C.; Mora, M.; Ruiz, J. R. Suzuki cross-coupling reaction over a palladium−pyridine complex immobilized on hydrotalcite. *Catal. Commun.* **2006**, *7* (12), 1025−1028.
(21) Cai, H.; Hillier, A. C.; Franklin, K. R.; Nunn, C. C.; Ward, M. D. Nanoscale Imaging of Molecular Adsorption. *Science* **1994**, *266* (5190), 1551.
(22) Winterbottom, J. M., Hydration and dehydration by heterogeneous catalysts. In *Catalysis*; Kemball, C., Dowden, D. A., Eds.; The Royal Society of Chemistry, 1981; Vol. *4*, pp 141−174.
(23) Meloni, D.; Sini, M. F.; Cutrufello, M. G.; Monaci, R.; Rombi, E.; Ferino, I. Characterization of the active sites in MgNiAl mixed oxides by microcalorimetry and test reaction. *J. Therm. Anal. Calorim.* **2012**, *108* (2), 783−791.
(24) Wang, W.; Xu, Z. X.; Guo, Z. L.; Jiang, C. F.; Chu, W. Layered double hydroxide and related catalysts for hydrogen production and a biorefinery. *Chin. J. Catal.* **2015**, *36* (2), 139−147.
(25) Kustrowski, P.; Chmielarz, L.; Bozek, E.; Sawalha, M.; Roessner, F. Acidity and basicity of hydrotalcite derived mixed Mg-Al oxides studied by test reaction of MBOH conversion and temperature programmed desorption of NH3 and CO2. *Mater. Res. Bull.* **2004**, *39* (2), 263−281.
(26) Newman, S. P.; Jones, W.; O'Connor, P.; Stamires, D. N. Synthesis of the 3R2 polytype of a hydrotalcite-like mineral. *J. Mater. Chem.* **2002**, *12* (2), 153−155.
(27) Obadiah, A.; Kannan, R.; Ravichandiran, P.; Ramasubbu, A.; Kumar, S. Nano hydrotalcite as a novel catalyst for biodiesel conversion. *Digest J. Nanomat. Biostr.* **2012**, *7*, 321−327.
(28) Sharninghausen, L. S.; Campos, J.; Manas, M. G.; Crabtree, R. H. Efficient selective and atom economic catalytic conversion of glycerol to lactic acid. *Nat. Commun.* **2014**, *5*, 5084.
(29) Vágvölgyi, V.; Palmer, S. J.; Kristóf, J.; Frost, R. L.; Horváth, E. Mechanism for hydrotalcite decomposition: A controlled rate thermal analysis study. *J. Colloid Interface Sci.* **2008**, *318* (2), 302−308.
(30) Wang, K.; Horlyck, J.; Finn, M.; Granollers Mesa, M.; Voutchkova-Kostal, A., Hydrotalcite-Supported Iridium NHCs as Robust Catalysts for Valorization of Glycerol to Lactic Acid. Manuscript in preparation. Manuscript in preparation. **2022**.
(31) Wagner, C. D.; Naumkin, A. V.; Kraut-Vass, A.; Allison, J. W.; Powell, C. J.; Rumble, J. R. J. NIST Standard Reference Database 20, Version 3.4 (web version). (http:/srdata.nist.gov/xps (accessed 2022-03-03).
(32) Freakley, S. J.; Ruiz-Esquius, J.; Morgan, D. J. The X-ray photoelectron spectra of Ir, IrO2 and IrCl3 revisited. *Surf. Interface Anal.* **2017**, *49* (8), 794−799.
(33) Zou, X.; Fan, H.; Tian, Y.; Zhang, M.; Yan, X. Chemical bath deposition of Cu2O quantum dots onto ZnO nanorod arrays for application in photovoltaic devices. *RSC Adv.* **2015**, *5* (30), 23401−23409.

https://doi.org/10.1021/acsomega.2c02593
ACS Omega XXXX, XXX, XXX−XXX